ECS Transactions, 64 (23) 11-17 (2015)
10.1149/06423.0011ecst ©The Electrochemical Society

Nanocomposite of TiO_2 Nanoparticles-Reduced Graphene Oxide with High-Rate Performance for Li-Ion Battery

Xiangcheng Sun[a], Yuefei Zhang[b], Lin Gu[c], Lilei Hu[a], Kun Feng[d], Zhongwei Chen[d] and Bo Cui[a]

[a]Department of Electrical and Computer Engineering and Waterloo Institute for Nanotechnology, University of Waterloo, Waterloo, Canada
[b]Institute of Microstructure and Property of Advanced Materials, Beijing University of Technology, Beijing, PR China
[c]Institute of Physics, Chinese Academy of Sciences, Beijing, PR China
[d]Department of Chemical Engineering, University of Waterloo, Waterloo, Canada

A simple and effective method is developed to synthesize the nanocomposites of anatase TiO_2 nanoparticles deposited on the reduced graphene oxide (TiO_2-RGO) sheets as anode materials for Li-ion battery applications. Structure analyses demonstrated that anatase TiO_2 nanoparticles were well dispersed onto the reduced graphene oxide nanosheets with chemical bonds. These TiO_2-RGO nanocomposites were electrochemically investigated in the coin-type cells versus metallic lithium, and the lithium storage performance of these nanocomposites showed the enhanced high-rate capabilities and good cycling stability. These improved electrochemical performance can be attributed mainly to efficient dispersion of TiO_2 nanocrystals on the surface of conductive RGO sheets, which makes these TiO_2-RGO nanocomposites practical for high-rate Li-ion battery applications.

Introduction

With rising interest in green electrode materials for new generation of Li-ion batteries with high power density and high rate capacity, TiO_2 has been regarded as a promising anode material for Li-ion batteries in recent years because of its environmental benignity, long cycle life, low cost, and good safety [1-3]. Moreover, the relatively high lithium insertion/extraction voltage of a TiO_2 anode (higher than 1.5 V vs Li^+/Li) can efficiently avoid the formation of solid-electrolyte interface (SEI) layers and lithium plating on the anode, which improves the safety of the batteries. TiO_2 is a typical Li^+ intercalation anode. The reaction can be expressed as $TiO_2 + xLi^+ + xe^- \Leftrightarrow Li_xTiO_2$ ($0 \leq x \leq 0.5$), while Li^+ ions insert/extract in the TiO_2 anode accompanied with the electron transfer between Ti(III) and Ti(IV). The reversible process provides a considerable capacity of 167.5 mA h g^{-1} with only a small volume variation (< 4%), which is critical for the high-rate capability and long-life cycling in the design of high-rate lithium-ion batteries. However, the practical application of the TiO_2 anode is still a challenge due to its low intrinsic electrical conductivity (10^{-12} S cm^{-1}), which leads to limited rate capability during reversible Li-ion insertion/extraction process [4]. In order to improve the electrochemical performance of TiO_2 materials, nanotechnology has been explored to provide increased reaction active sites and short diffusion lengths for both electron and Li-ion transport [5-6]. A variety of approaches have been developed to increase the electronic conductivity of the TiO_2, such as adding conductive agents [7] or using

conductive coating [8]. So far, the most effective way to enhance its electrical conductivity is by surface carbon coating, which can maintain an excellent electronic contact among TiO_2 particles and hence enhance the high-rate reactions without the loss of active materials. Graphene and graphene oxide (GO) have been regarded as an ideal carbon nanostructure to improve the rate capability of TiO_2 owing to its superior electronic conductivity and large surface area (e.g., 2630 m^2/g) [9]. It was reported that TiO_2-graphene nanocomposite exhibited a high capacity and excellent rate capability in the enlarged potential window of 0.01-3.0 V since the graphene acts not only as a conductive agent but also as a lithium storage material [10]. In this work, well-distributed TiO_2 nanoparticles deposited on reduced graphene oxide (RGO) was synthesized through one-step hydrothermal method using commercial anatase TiO_2 powders as the precursors. Compared with the reported hydrothermal-solvothermal routes, the current preparation was performed without high-temperature calcination and addition of any surfactants. The obtained TiO_2-RGO composites possessed a highly crystallized spherical morphology, the electrochemical performance of TiO_2-RGO composites can be remarkably improved in terms of good high-rate performance and cycling stability. The synthetic route for TiO_2-RGO composites is facile and nontoxic, therefore can be readily scaled up.

Experimentals

Firstly, graphene oxides were synthesized via modified Hummers methods as described elsewhere [11,12]. Briefly, 25 mg of graphene oxide was added to 75 mL deionized water, then 5 mL of 1.5 M sodium hydroxide solution was added to obtain a colloidal solution that was sonicated for 30 min. Such a colloidal solution was subsequently mixed with 50 mg commercial TiO_2 powders (ca. 25 nm, Fisher Scientific Inc.) by high-speed stirring for 1 h. The resulting solution was put into an autoclave and heated at 180°C for 10h. When the reduction reaction was finished, the as-synthesized TiO_2-RGO composites were isolated by centrifugation, washed with ethanol and deionized water several times, and dried at 80°C for 2h.

Structures were characterized by X-ray diffraction (XRD) on a Bruker D8 Advance X-ray diffractometer using Cu Kα radiation (λ=1.5418 nm). Transmission electron microscopy (TEM), high-resolution transmission electron microscope (HRTEM) and selected-area electron diffractions (SAED) were performed on a JEOL-2010F TEM operated at 200 kV to characterize the morphology, size and the crystalline structure of the samples.

To investigate the lithium storage performances of the TiO_2-RGO nanocomposite, working electrodes were assembled in cells and tested in the voltage range of 1.0 - 3.0 V. The working electrodes were prepared from a mixture of 75 wt.% active materials, 15 wt.% Super P carbon black, and 10 wt.% polyvinylidene (PVDF) binder in an N-methyle-2-pyrrolidone (NMP) solvent. Highly pure lithium foil was used as the counter electrode. The electrolyte used was 1 M LiPF6 dissolved in the mixture of ethyl carbonate (EC) and dimethyl carbonate (DMC) with the volume ratio of 1:1. The coin cells were assembled in argon-filled glove box. The cells were galvanostatically discharged and charged in the potential windows (1.0-3.0 V) using a Battery Testing System. Cyclic voltammetry (CV) were carried out using coin cells (CR2032) on a LAND-CT2001A battery-testing system over the potential range of 1.0-3.0 V vs. Li/Li^+ at a scanning rate of 0.5 mV s^{-1}.

Results and discussion

X-ray diffraction (XRD) was applied to identify the crystalline phase of TiO_2-RGO nanocomposites, as shown in Figure 1.

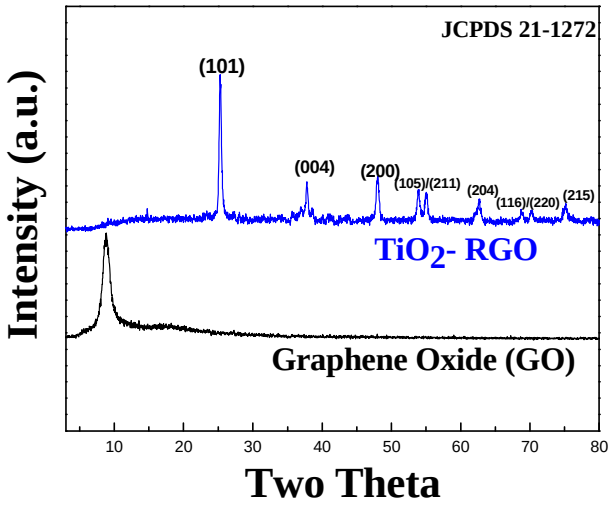

Figure 1. X-ray diffraction patterns of graphene oxide (GO) and TiO_2-RGO composites.

The characteristic peak (~10°) of GO can be clearly observed in the XRD pattern, corresponding to the (001) plane of GO. After the hydrothermal reduction, this peak entirely disappeared, indicating that the –OH, C=O bond and –COOH groups have been removed from GO to a great extent. All the XRD diffraction peaks (101), (004), (200), (105) and (211) of TiO_2-RGO can be well assigned to anatase phase TiO_2 that indexed with the Joint Committee on Powder Diffraction Standards (JCPDS) Card File No. 21-1272 [13].

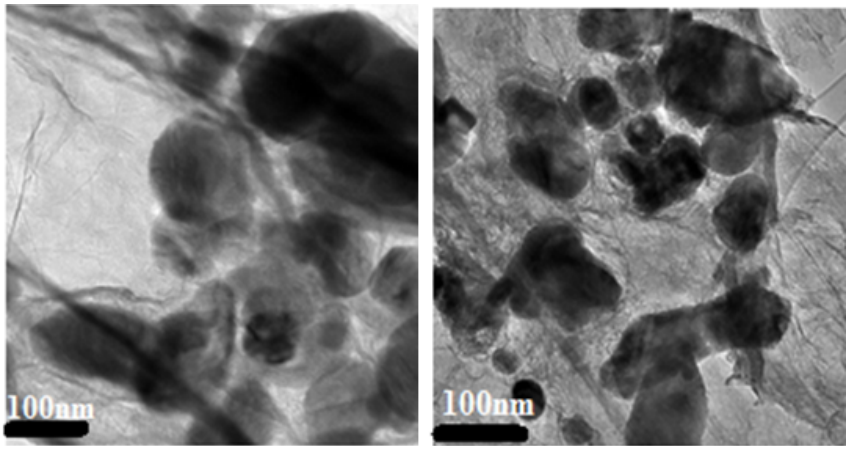

Figure 2. Transmission electron microscopy (TEM) images of the TiO_2-RGO composites.

The morphology investigations from TEM images in Figure 2 showed both spherical particles aggregates (e.g., 100 nm) and singles spherical particles (e.g., 25 nm) are well dispersed on the RGO nanosheets, which indicates that spherical TiO_2 particles and RGO nanosheets are strongly chemically bonded rather than loosely aggregated.

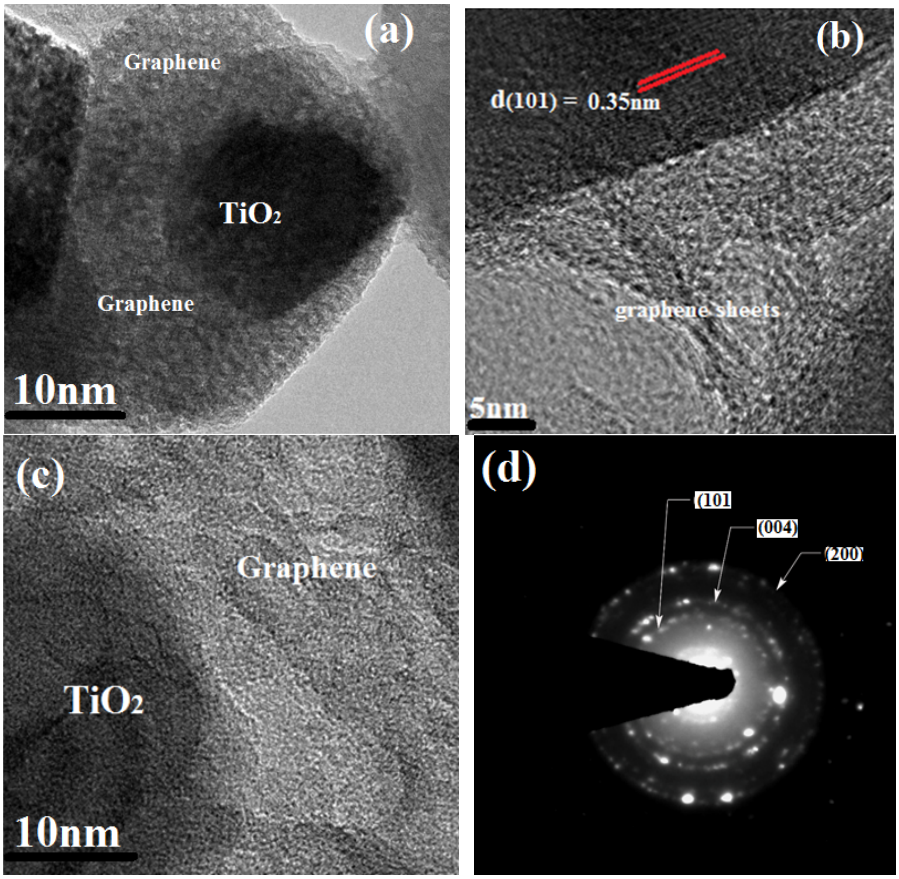

Figure 3. HRTEM images (a-c) and (d) SAED patterens for the TiO_2–RGO nanocomposites.

HR-TEM images in Figure 3(a-c) further confirm the morphology characteristics of the TiO_2 nanoparticles. Well-crystallized TiO_2 nanoparticles were dispersed onto reduced graphene nanosheets, and some individual TiO_2 spherical nanoparticle has retained the diameter of 25 nm. This suggests a good dispersion of reduced graphene nanosheets during the hydrothermal synthesis, which is great beneficial to the rate performance. The crystalline lattice distance in HR-TEM images is ~0.35 nm, corresponding to characteristic of the (101) planes of anatase TiO_2 phase [14]. The SAED pattern (Figure 3d) of these nanoparticles in the composites reveals the lattice spacings corresponding to the (1 0 1), (0 0 4) and (2 0 0) diffractions of the anatase phase [15].

To investigate the electrochemical performances of these TiO_2-RGO composites, the samples were assembled as anodes for LIBs, and were comprehensively evaluated in half-cell batteries. Figure 4 presents the three galvanostatic discharging/charging curves of the sample at 0.5 C rate within a voltage window of 1.0-3.0 V. The sample displayed a discharge voltage plateau at 1.76 V and a charge voltage plateau at 1.91 V, which are characteristic of anatase TiO_2 [16]. By sharp contrast, TiO_2-RGO composites exhibited a higher discharge capacity of over 200 mAh g^{-1} at the initial cycle, which are higher than the theoretical capacity of bulk titania (167.5 mA h g^{-1}) with the maximum lithium insertion of 0.5 ($Li_{0.5}TiO_2$) during the redox reaction. The irreversible capacity after initial cycle is ascribed to the formation of solid-electrolyte interface (SEI) films.

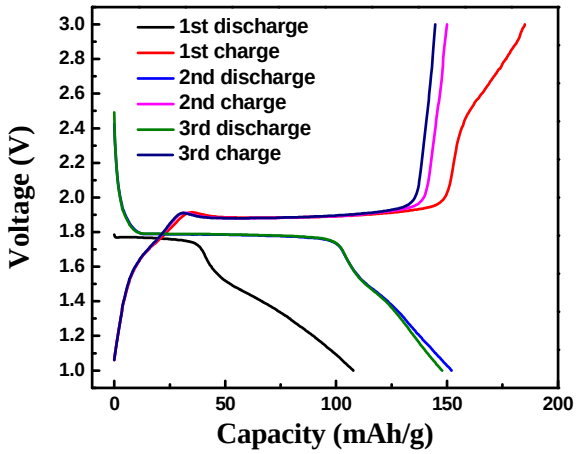

Figure 4. The galvanostatic discharge/charge profiles of TiO_2-RGO composites at 0.5 C.

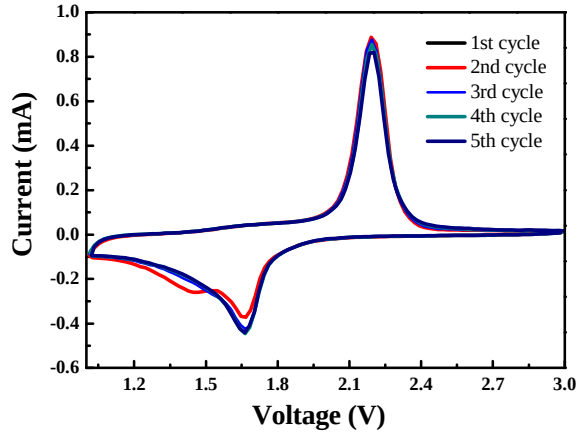

Figure 5. Cyclic voltammograms of TiO_2-RGO composites at the scan rate of 0.5 mV s^{-1}.

To better understand the high-rate electrochemical behaviors of TiO_2-RGO composites, cyclic voltammogram (CV) was performed between 0 and 3.0 V at a scanning rate of 0.5 mV s^{-1}, as shown in Figure 5. Consistent with galvanostatic discharging/charging curves, two distinct peaks can be observed at ~1.7 and 2.1 V during the cathodic and anodic scan, respectively. These two peaks can be regarded as the signature of the lithium insertion/extraction processes in the anatase framework [17, 18], and such a pair of redox peaks corresponds to the reversible biphasic transition between tetragonal anatase and orthorhombic Li_xTiO_2 [19, 20]. The good symmetry of the redox peaks after 5 cycles further reveals the excellent rate capability of the TiO_2-RGO composites.

The excellent cycling stability at 1C rate was demonstrated in Figure 6. It is also observed the coulombic efficiency is approximately 100% with an excellent cycling stability even in the 50th cycle. Approximately 99% of its initial charge/discharge is retained after 50 discharge/charge cycles, and almost no capacity fading was occurred, indicating very good reversibility. In short, our anatase TiO_2-RGO nanocompsoites exhibit a highly crystalline spherical morphology, high-rate performance and excellent cycle life for lithium storage.

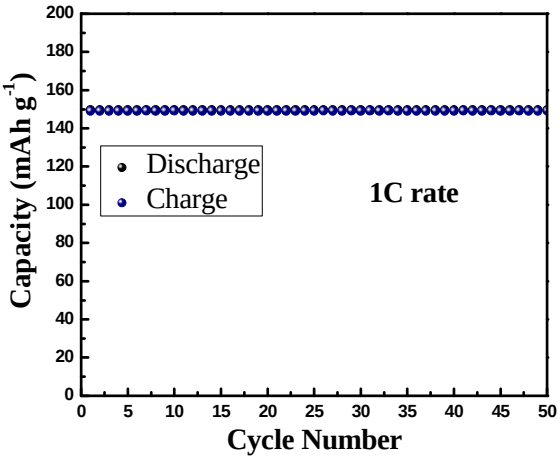

Figure 6. Cycling performance of the TiO_2-RGO composites at 1 C rate.

Such a high-rate capability and cycling stability can be attributed to the unique nanostructure of TiO_2-RGO composites as well as the existence of graphene network as a conducting agent that greatly improves the electrical conductivity of the nanocomposite [15-20]. More importantly, graphene sheets with a large surface area are able to serve as substrates that effectively inhibit the aggregation of TiO_2 nanoparticles, which remarkably raises the homogeneity of the Li ion insertion/extraction and enables fast and efficient diffusion of lithium ions [10, 19, 20].

In brief, the excellent performance of our TiO_2-RGO nanocomposites can be attributed to several possible factors [10, 19-23]. First, for anastase TiO_2 nano-sized particles, more than 0.5 Li^+ per TiO_2 can be inserted/extracted in the discharge-charge process. The small nanoparticles can provide short path lengths for electron and Li-ion transport during the Li-ion insertion/extraction process [20], resulting in excellent rate capability and cyclic stability. Second, reduced graphene oxide nanosheets have significant disorder/defects, this can facilitate electron transfer and contribute to the extra lithium storage capacity, which enhances the overall capacity. Third, during the cycling, the anatase crystallized TiO_2 may transform increasingly to become amorphous, which makes much more accessible active sites available for Li^+ ion insertion. Lastly, most TiO_2 nanocrystal were dispersed onto RGO nanosheets with minimal TiO_2 agglomeration and RGO stacking, which leads to large surface area during lithium insertion/extraction.

Conclusions

The hydrothermal synthesis provides a facile and scalable approach to deposit anatase TiO_2 nanoparticles onto RGO sheets using both commercial TiO_2 powders and graphene oxide (GO) as precursors. The TiO_2-RGO composites involve one-step hydrothermal treatment without any surfactant or high-temperature calcinations. Structure analyses (XRD and TEM) demonstrated that anatase TiO_2 nanoparticles were well dispersed onto RGO nanosheets. These TiO_2-RGO nanocomposites have improved lithium storage with an enhanced rate capabilities and cycling stability at high charge/discharge rate. These improved electrochemical performance can be mainly attributed to the fact that conductive graphene nanosheets attached on TiO_2 nanoparticles provide high electrical conductivity and large surface area for fast lithium storage. This work is favorable for

exploring advanced TiO_2-based composites as anode materials for high-rate Li-ion batteries.

Acknowledgments

Y. Z. acknowledges the research supports from Beijing Natural Science Foundation (No. 2132014) at China. Special thanks to Dr. Jun He's team group for the helps in electrochemical testing at Central South University (CSU) of China.
The financial supports from Natural Sciences and Engineering Research Council of Canada (NSERC), University of Waterloo President's Award and Waterloo Institute for Nanotechnology (WIN) Nanofellowships are greatly appreciated.

References

1. Z. Yang, D. Choi, S. Kerisit, K. M. Rosso, D. Wang, J. Zhang, G. Graff, and J. Liu, *J. Power Sources* , 1**92**, 588 (2009).
2. P. Kubiak, T. Fröschl, N. Hüsing, U. Hörmann, U. Kaiser, R. Schiller, C. K. Weiss, K. Landfester, and M. Wohlfahrt-Mehrens, *Small*, **7**, 1690 (2011).
3. J. S. Chen and X.W. Lou, *Electrochem. Commun*., **11,** 2332 (2009).
4. S. Bach, J. P. Pereira-Ramos, P. Willman, *Electrochim. Acta*, **55**, 4952 (2010).
5. Y. H. Jin, S. H. Lee, H.W. Shim, K.H. Ko, and D.W. Kim, *Electrochim. Acta*, **55**, 7315 (2010).
6. F. Wu, Z. Wang, X. Li, and H. Guo, *J. Mater. Chem*., **21,** 12675 (2011).
7. Y. Wang, T. Chen, and Q. Mu, *J. Mater. Chem*., **21,** 6006 (2011).
8. J. S. Chen, H. Liu, S. Z. Qiao, and X.W. Lou, *J. Mater. Chem*., **21,** 5687 (2011).
9. N. Li, G. Liu, C. Zhen, F. Li, L. Zhang, and H. M. Cheng, *Adv. Funct. Mater*., **21**, 1717 (2011).
10. D. D. Cai, P. C. Lian, X. F. Zhu, S. Z. Liang, W. S. Yang, and H. H. Wang, *Electrochem. Acta*, **74**, 65 (2012).
11. W. S. Hummers Jr. and R. E. Offeman, *J. Am. Chem. Soc*., **80,** 1339 (1958).
12. S. Guo and S. Dong, *Chem. Soc. Rev.*, **40**, 2644 (2011).
13. J. S. Chen, Y. L. Tan, C. M. Li, Y. L. Cheah, D. Y. Luan, S. Madhavi, F. Y. C. Boey, L. A. Archer, and X. W. Lou, *J. Am. Chem. Soc*., **132**, 612 (2010).
14. L. Bai, F. Fang, Y.Y. Zhao, Y.G. Liu, J. P. Li, G.Y. Huang, and H. Y. Sun, *RSC Adv*., **4**, 43039 (2014).
15. H.T. Tao, L. Z. Fan, X. Q.Yan, and X. H. Qu, *Electrochim. Acta*, **69**, 328 (2012).
16. Y. H. Ding, P. Zhang, H. M. Ren, Q. Zhuo, Z. M. Yang, and Y. Jiang, *Mater. Res. Bull*., **46**, 2403 (2011)
17. S. J. Ding, J. S. Chen, D. Y. Luan, F. Y. C. Boey, S. Madhavi, and X. W. Lou, *Chem. Commun*., **47**, 5780 (2011).
18. D. Wang, D. Choi, J. Li, Z. Yang, Z. Nie, and R. Kou et al, *ACS Nano*, **3**, 907 (2009).
19. H. Wang, Z. Lu, L. Xi, R. Ma, C. Wang, J. A. Zapien, and I. Bello, *ACS Appl. Mater. Inter*., **4**, 1608 (2012).
20. X. Xin, X. Zhou, J. Wu, X. Yao and Z. P. Liu, *ACS Nano*, **6**, 11035 (2012).
21. M. Zhen, X. Guo, G. Gao, Z. Zhou and L. Liu, *Chem. Commun*., **50**, 11915 (2014).
22. H. Han, T. Song, J. Y. Bae, L.F. Nazar, H. Kim, and U. Paik, *Energy Environ. Sci*., **4**, 4532 (2011).
23. T. Hu, X. Sun, H. Sun, M. P. Yu, F.Y. Lu, and J. Lian, *Carbon*, **51**, 322 (2013).